Biogeosciences, 13, 3701–3715, 2016
www.biogeosciences.net/13/3701/2016/
doi:10.5194/bg-13-3701-2016

Biogeosciences Open Access EGU

Ocean acidification in the subpolar North Atlantic: rates and mechanisms controlling pH changes

Maribel I. García-Ibáñez[1], Patricia Zunino[2], Friederike Fröb[3], Lidia I. Carracedo[4], Aida F. Ríos[†], Herlé Mercier[5], Are Olsen[3], and Fiz F. Pérez[1]

[1]Instituto de Investigaciones Marinas, IIM-CSIC, Vigo, E36208, Spain
[2]Ifremer, Laboratoire d'Océanographie Physique et Spatiale, UMR 6523 CNRS/Ifremer/IRD/UBO, Ifremer Centre de Brest, Plouzané, CS 10070, France
[3]Geophysical Institute, University of Bergen and Bjerknes Centre for Climate Research, Bergen, N5007, Norway
[4]Faculty of Marine Sciences, University of Vigo, Vigo, E36200, Spain
[5]CNRS, Laboratoire d'Océanographie Physique et Spatiale, UMR 6523 CNRS/Ifremer/IRD/UBO, Ifremer Centre de Brest, Plouzané, CS 10070, France
[†]deceased

Correspondence to: Maribel I. García-Ibáñez (maribelgarcia@iim.csic.es)

Received: 24 February 2016 – Published in Biogeosciences Discuss.: 29 February 2016
Revised: 24 May 2016 – Accepted: 27 May 2016 – Published: 23 June 2016

Abstract. Repeated hydrographic sections provide critically needed data on and understanding of changes in basin-wide ocean CO_2 chemistry over multi-decadal timescales. Here, high-quality measurements collected at twelve cruises carried out along the same track between 1991 and 2015 have been used to determine long-term changes in ocean CO_2 chemistry and ocean acidification in the Irminger and Iceland basins of the North Atlantic Ocean. Trends were determined for each of the main water masses present and are discussed in the context of the basin-wide circulation. The pH has decreased in all water masses of the Irminger and Iceland basins over the past 25 years with the greatest changes in surface and intermediate waters (between -0.0010 ± 0.0001 and -0.0018 ± 0.0001 pH units yr^{-1}). In order to disentangle the drivers of the pH changes, we decomposed the trends into their principal drivers: changes in temperature, salinity, total alkalinity (A_T) and total dissolved inorganic carbon (both its natural and anthropogenic components). The increase in anthropogenic CO_2 (C_{ant}) was identified as the main agent of the pH decline, partially offset by A_T increases. The acidification of intermediate waters caused by C_{ant} uptake has been reinforced by the aging of the water masses over the period of our analysis. The pH decrease of the deep overflow waters in the Irminger basin was similar to that observed in the upper ocean and was mainly linked to the C_{ant} increase, thus reflecting the recent contact of these deep waters with the atmosphere.

1 Introduction

The oceanic uptake of a fraction of the anthropogenic CO_2 (i.e. C_{ant}; CO_2 released from humankind's industrial and agricultural activities) has resulted in long-term changes in ocean CO_2 chemistry, commonly referred to as ocean acidification (OA; e.g. Caldeira and Wickett, 2003, 2005; Raven et al., 2005; Doney et al., 2009; Feely et al., 2009). The changes in the ocean CO_2 chemistry result in declining pH and reduced saturation states for $CaCO_3$ minerals (e.g. Bates et al., 2014). The average pH ($-\log_{10}[H^+]$) of ocean surface waters has decreased by about 0.1 pH units since the beginning of the industrial revolution (1750), and based on model projections we expect an additional drop of 0.1–0.4 by the end of this century, even under conservative CO_2 emission scenarios (Caldeira and Wickett, 2005; Orr, 2011; Ciais et al., 2013). The rate of change in pH is at least a hundred times faster than at any time since the last ice age (Feely et al., 2004; Raven et al., 2005), clearly outpacing natural processes in ocean chemistry that have occurred in the past due to geological processes (Raven et al., 2005). These changes

in ocean CO_2 chemistry will most likely have adverse effects on organisms, particularly calcifying ones; ecosystems (e.g. Langdon et al., 2000; Riebesell et al., 2000; Pörtner et al., 2004) and major marine biogeochemical cycles (e.g. Gehlen et al., 2011; Matear and Lenton, 2014).

The global ocean has absorbed $\sim 30\,\%$ of the C_{ant} emitted to the atmosphere between 1750 and the present (Sabine et al., 2004; Khatiwala et al., 2013; DeVries, 2014; Le Quéré et al., 2015). This C_{ant} is not evenly distributed throughout the oceans (Sabine et al., 2004), but enters the interior ocean preferentially in regions of deep convective overturning and subduction (Maier-Reimer and Hasselmann, 1987; Sarmiento et al., 1992; Lazier et al., 2002). This explains why the meridional overturning circulation (MOC) makes the North Atlantic Ocean one of the most important C_{ant} sinks of the global ocean, storing 25 % of the global oceanic C_{ant} (Sabine et al., 2004; Khatiwala et al., 2013) despite being only 11 % of the global ocean volume (Eakins and Sharman, 2010). The MOC transports C_{ant}-laden surface waters from the Equator to the northern North Atlantic Ocean (e.g. Wallace, 2001; Anderson and Olsen, 2002; Olsen et al., 2006; Zunino et al., 2015), where deep water formation provides a pathway for C_{ant} into the interior ocean (Lazier et al., 2002; Pérez et al., 2008, 2013; Steinfeldt et al., 2009). Being regions close to deep water formation areas and where water mass transformation occurs (Sarafanov et al., 2012; García-Ibáñez et al., 2015), the Irminger and Iceland basins are geographically well placed to monitor temporal changes in the Atlantic MOC (Mercier et al., 2015) and to determine the rates of C_{ant} penetration to the deep ocean and its consequence for OA.

In this paper, we examine high-quality direct measurements of ocean CO_2 chemistry from twelve cruises conducted across the Irminger and Iceland basins between 1991 and 2015. Previous studies focused on C_{ant} uptake and its storage and effect on pH in the Irminger and Iceland basins (e.g. Pérez et al., 2008; Olafsson et al., 2009; Bates et al., 2012; Vázquez-Rodríguez et al., 2012b). Here we quantify the pH change for a 25-year period and identify its chemical and physical drivers by decomposing the observed pH change into five numerically estimated factors (temperature, salinity, alkalinity, anthropogenic CO_2 and non-anthropogenic CO_2), all based on direct measurements.

2 Materials and methods

2.1 Datasets

2.1.1 Cruise Information

We used data from twelve cruises along the same track across the Irminger and Iceland basins, with the cruise dates spanning 25 years (1991–2015; Table 1, Fig. 1a). The bottle data were accessed from the merged data product of the

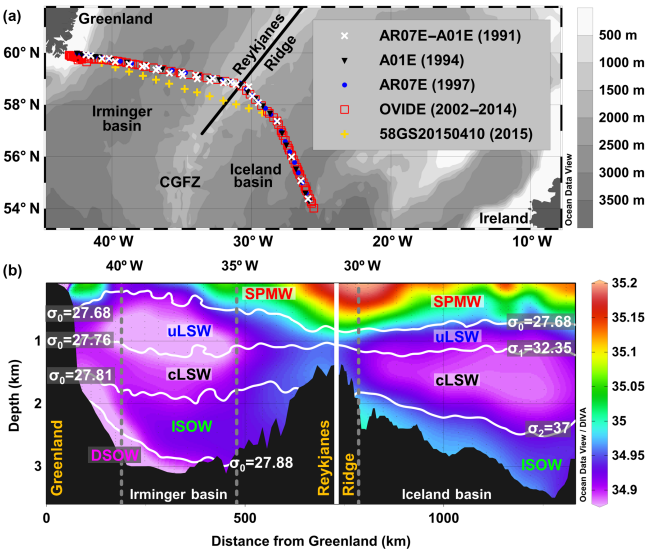

Figure 1. (a) Sampling locations of the twelve cruises used in this study (1991–2015) plotted on bathymetry (500 m intervals). The black line shows the boundary between the Irminger and the Iceland basins constituted by the Reykjanes Ridge. CGFZ stands for Charlie–Gibbs Fracture Zone. **(b)** Limits of the layers and basins considered in this study plotted on top of the salinity distribution for the 2004 cruise. The isopycnals delineating the layers are defined by potential density (referenced to 0 dbar, σ_0; 1000 dbar, σ_1; and 2000 dbar, σ_2; all in kg m^{-3}) and the vertical white line is the limit (Reykjanes Ridge) between the Irminger (left) and Iceland basins (right). The dashed vertical lines represent the longitude axis marks. The layer acronyms are Subpolar Mode Water (SPMW), upper and classical Labrador Sea Water (uLSW and cLSW, respectively), Iceland–Scotland Overflow Water (ISOW) and Denmark Strait Overflow Water (DSOW).

Global Data Analysis Project version 2 (GLODAPv2; Olsen et al., 2016) at http://cdiac.ornl.gov/oceans/GLODAPv2, except for more recent data collected during the OVIDE 2012 and 2014 cruises and the 2015 cruise (58GS20150410). The data of the 1991 cruises (64TR91_1 and 06MT18_1) were merged and treated as a single cruise.

2.1.2 Ocean CO_2 chemistry measurements

The twelve cruises selected for our study have high-quality measurements of the seawater CO_2 system variables (Table 1). Total alkalinity (A_T) was analysed by potentiometric titration and determined by developing either a full titration curve (Millero et al., 1993; Dickson and Goyet, 1994; Ono et al., 1998) or from single point titration (Pérez and Fraga, 1987; Mintrop et al., 2000) and was calibrated with certified reference materials (CRMs) with an overall accuracy of 4 µmol kg^{-1}. For samples without direct A_T measurements, A_T was estimated using a 3-D moving window multilinear regression algorithm (3DwMLR), using potential temperature (θ), salinity, nitrate, phosphate, silicate and

Table 1. List of hydrographic cruises used in this study (Fig. 1a). P.I. denotes principal investigator, #St the number of stations used here and "Measurements" refers to the seawater CO_2 system measurements performed during these cruises.

Cruise name	Expocode	Month yr^{-1}	Vessel	P.I.	#St	Measurements	Reference
AR07E	64TR91_1	04–05/1991	*Tyro*	H. M. van Aken	12	DIC	Stoll et al. (1996)
A01E	06MT18_1	09/1991	*Meteor*	J. Meincke	15	A_T and DIC	Meincke and Becker (1993)
A01E	06MT30_3	11–12/1994	*Meteor*	J. Meincke	27	DIC	Koltermann et al. (1996)
AR07E	06MT39_5	08–09/1997	*Meteor*	A. Sy	32	DIC	Rhein et al. (2002)
OVIDE 2002	35TH20020610	06–07/2002	*Thalassa*	H. Mercier	38	pH and A_T	Lherminier et al. (2007)
OVIDE 2004	35TH20040604	06–07/2004	*Thalassa*	T. Huck	56	pH and A_T	Lherminier et al. (2010)
OVIDE 2006	06MM20060523	05–06/2006	*Maria S. Merian*	P. Lherminier	44	pH and A_T	Gourcuff et al. (2011)
OVIDE 2008	35TH20080610	06–07/2008	*Thalassa*	H. Mercier	45	pH and A_T	Mercier et al. (2015)
OVIDE 2010	35TH20100610	06/2010	*Thalassa*	T. Huck; H. Mercier	46	pH and A_T	Mercier et al. (2015)
CATARINA*	29AH20120623	06–07/2012	*Sarmiento de Gamboa*	A. F. Ríos	44	pH and A_T	This work
GEOVIDE*	35PQ20140517	05–06/2014	*Pourquoi Pas?*	G. Sarthou	31	pH and A_T	This work
58GS20150410	58GS20150410	04–05/2015	*G.O. Sars*	A. Olsen	10	A_T and DIC	Fröb et al. (2016)

* Both CATARINA (http://catarina.iim.csic.es/en) and GEOVIDE (http://www.geovide.obs-vlfr.fr) cruises contain the OVIDE section (http://www.umr-lops.fr/Projets/Projets-actifs/OVIDE) and in the study are referred to as OVIDE 2012 and 2014, respectively.

oxygen as predictor parameters (Velo et al., 2013). The total dissolved inorganic carbon (DIC) samples were analysed with coulometric titration techniques (Johnson et al., 1993) and calibrated with CRMs, achieving an overall accuracy of 2 µmol kg^{-1}. For the cruises for which direct DIC measurements had not been performed, it was computed from A_T and pH using the thermodynamic equations of the seawater CO_2 system (Dickson et al., 2007) and the CO_2 dissociation constants of Mehrbach et al. (1973) refitted by Dickson and Millero (1987). These calculated DIC values have an associated uncertainty of 4 µmol kg^{-1}, calculated by random propagation of the reported A_T and pH accuracies. pH was determined at 25 °C and 1 atm with a spectrophotometric method (Clayton and Byrne, 1993) using diode array spectrophotometers and m-cresol purple as an indicator. The spectrophotometric pH determination has a typical precision of 0.0002–0.0004 pH units (Clayton and Byrne, 1993; Liu et al., 2011). However, Carter et al. (2013) reported an inherent uncertainty of spectrophotometric pH determinations of 0.0055 pH units, associated to the tris-buffer used for calibration. When direct pH measurements were not performed, pH was computed from A_T and DIC using the thermodynamic equations of the seawater CO_2 system (Dickson et al., 2007) and the CO_2 dissociation constants of Mehrbach et al. (1973) refitted by Dickson and Millero (1987). For these calculated pH values, we estimated an uncertainty of 0.006 pH units by random propagation of the reported A_T and DIC accuracies. A_T values differing by more than two times the standard deviation (7 µmol kg^{-1}) of the difference between measured A_T and 3DwMLR-predicted A_T were replaced with the predicted A_T value. Note that the effect of A_T corrections on pH trends is negligible, since A_T corrections of 4 µmol kg^{-1} lead to pH changes lower than a thousandth. The pH values reported here are at in situ conditions (of temperature and pressure) and on the total scale ($pH_{T_{is}}$).

2.1.3 Anthropogenic CO_2 (i.e. C_{ant}) estimation

C_{ant} concentrations were estimated using the back-calculation method φC_T^0 (Pérez et al., 2008; Vázquez-Rodríguez, 2009a) that has previously been applied for the entire Atlantic Ocean (Vázquez-Rodríguez et al., 2009b). Back-calculation methods determine C_{ant} for any sample in the water column as the difference between DIC concentration at the time of the measurement and the DIC concentration it would have had in preindustrial times. Following Gruber et al. (1996), this is represented as the difference in preformed DIC between the time of observation and the preindustrial:

$$C_{ant} = DIC_{meas} - \Delta C_{bio} - DIC_{preind} - \Delta C_{diseq}, \quad (1)$$

where the preformed DIC for the time of observation is represented as the measured DIC (DIC_{meas}) minus any DIC added to the water due to organic matter remineralisation and calcium carbonate dissolution (ΔC_{bio}). The preindustrial preformed concentration is represented by the DIC concentration the water would have if in equilibrium with the preindustrial atmosphere (DIC_{preind}) minus any offset from such an equilibrium value, known as the disequilibrium term (ΔC_{diseq}). The procedure requires DIC and A_T as input parameters, and the empirical parameterisation of the preformed A_T (A_T^0) for the computation of the calcium carbonate dissolution and of the ΔC_{diseq} term (Vázquez-Rodríguez et al., 2012a). The A_T^0 is based on the concept of potential alkalinity ($PA_T = A_T + NO_3 + PO_4$) and is defined as $A_T^0 = PA_T - (NO_3^0 + PO_4^0)$ (Vázquez-Rodríguez et al., 2012a), where NO_3^0 and PO_4^0 are the preformed nitrate and phosphate concentrations, respectively. NO_3^0 and PO_4^0 are determined as $NO_3^0 = NO_3 - AOU / R_{ON}$ and $PO_4^0 = PO_4 - AOU / R_{OP}$. In the former equations AOU (apparent oxygen utilisation) is the difference between the saturated concentrations of oxygen calculated using the equations of Benson and Krause (1984) and the measured con-

centrations of oxygen, while R_{ON} and R_{OP} are the Redfield ratios proposed by Broecker (1974).

The φC_T^0 method presents two main advantages relative to the previous method proposed by Gruber et al. (1996). First, the spatiotemporal variability of A_T^0 is taken into account. And second, the parameterisations of A_T^0 and ΔC_{diseq} are determined using the subsurface layer as a reference (Vázquez-Rodríguez et al., 2012a), where the age of the water parcel, and therefore its C_{ant} concentration, is estimated using CFC measurements (Waugh et al., 2006). The overall uncertainty of the φC_T^0 method has been estimated at 5.2 µmol kg^{-1} (Pérez et al., 2008; Vázquez-Rodríguez, 2009a).

2.1.4 Trend uncertainty

The uncertainties and reproducibilities of the analysis and calculation methods were determined from the deep waters sampled at the Iberian Abyssal Plain during the seven repetitions of the OVIDE line, since these waters are expected to be in near steady state. The standard deviations of those samples for each cruise (Table 2) were taken as an estimate of the uncertainty at each cruise. The uncertainties of the AOU, A_T and $pH_{T_{is}}$ for the seven cruises were similar. The standard deviations of C_{ant} (1.2–1.6 µmol kg^{-1}) and $pH_{T_{is}}$ (0.002–0.003 pH units) for each of the seven cruises are lower than the inherent uncertainty of the φC_T^0 estimates (5.2 µmol kg^{-1}) and the accuracy of the spectrophotometric pH measurements (0.0055 pH units), which provides confidence that these data are suitable for trend determination. The standard deviations of the C_{ant} estimates are rather similar to those from other regions where C_{ant} has been compared across many cruises (i.e. 2.4 µmol kg^{-1} in the South Atlantic Ocean, Ríos et al. (2003); 2.7 µmol kg^{-1} in the equatorial Atlantic Ocean, 24° N, Guallart et al. (2015); and 2.7 µmol kg^{-1} reported from a transect along the western boundary of the Atlantic Ocean from 50° S to 36° N, Ríos et al., 2015). The standard deviations of the mean values of the Iberian Abyssal Plain samples across all (last row of Table 2) were taken as an estimate of the reproducibility of the methodologies. The high reproducibility of the pH measurements, at an order of magnitude higher than the uncertainty (0.0055 pH units, Carter et al., 2013), is suggestive of high quality data. Using these standard deviations for the seven cruises, and taking into account the 25 years considered in this study, the threshold of detectability of pH trends at 95 % of confidence is 0.00012 pH units yr^{-1}, which renders confidence to the estimated trends.

2.2 Water mass characterisation

Changes in ocean CO_2 chemistry were determined for the main water masses in the Irminger and Iceland basins. These are (1) Subpolar Mode Water (SPMW), (2) upper and classical Labrador Sea Water (uLSW and cLSW, respectively), (3) Iceland–Scotland Overflow Water (ISOW) and (4) Denmark Strait Overflow Water (DSOW; Fig. 1b). The layers defining the water masses were delimited using potential density following Azetsu-Scott et al. (2003), Kieke et al. (2007), Pérez et al. (2008) and Yashayaev et al. (2008). The advantage of working in layers is the relatively low variability of the physical and chemical properties within the layers, allowing us to assume linearity in the ocean CO_2 system.

To better determine the limits between layers and the average value of each variable in each layer, cruise bottle data were linearly interpolated onto each dbar before determining average variable values, an improvement with respect to the previous approaches of Pérez et al. (2008, 2010) and Vázquez-Rodríguez et al. (2012b). Then, the interpolated profiles were averaged over each density layer, defined in Figure 1b. Finally, the average values in each density layer were determined for each cruise taking into account the thickness of the layer and the separation between stations. The exception comes with $pH_{T_{is}}$, which is pressure sensitive and for which we needed to define a unique reference pressure to remove pressure effects due to varying sampling strategies. $pH_{T_{is}}$ was calculated using the layer average values of DIC and A_T for the considered year but using the time-averaged pressure of the layer over the studied time period as reference pressure. To reduce the influence of seasonal differences in sampling on the interannual trends, only samples with pressure ≥ 75 dbar were considered. The 75 dbar level was determined by the depth of the seasonal nutrients drawdown along the section. The average values of the variables for each layer and their standard deviations can be found in the Supplement (Table S1).

2.3 pH deconvolution

Changes in ocean pH may be brought about by changes in in situ temperature (T_{is}), salinity (S), A_T and/or DIC. Changes in the latter may be brought about by C_{ant} uptake or by natural processes (C_{nat}) such as remineralisation. C_{nat} is determined as the difference between measured DIC and estimated C_{ant}. Changes in temperature and salinity influence the equilibrium constants of the oceanic CO_2 system. Additionally, changes in salinity influence the borate concentration, which is taken into account by the relationship proposed by Uppström (1974).

To estimate how much each of these five factors have contributed to the observed change in pH, we assumed linearity and decomposed the observed pH changes into these potential drivers:

$$\left(\frac{\mathrm{d}pH_{T_{is}}}{\mathrm{d}t}\right)_{total} = \frac{\partial pH_{T_{is}}}{\partial T_{is}}\frac{\mathrm{d}T_{is}}{\mathrm{d}t} + \frac{\partial pH_{T_{is}}}{\partial S}\frac{\mathrm{d}S}{\mathrm{d}t} + \frac{\partial pH_{T_{is}}}{\partial A_T}\frac{\mathrm{d}A_T}{\mathrm{d}t} + \frac{\partial pH_{T_{is}}}{\partial DIC}\left(\frac{\mathrm{d}C_{ant}}{\mathrm{d}t} + \frac{\mathrm{d}C_{nat}}{\mathrm{d}t}\right). \quad (2)$$

To estimate $\frac{\partial pH_{T_{is}}}{\partial var}$ (where "var" refers to each of the drivers: T_{is}, S, A_T and DIC) we calculated a $pH_{T_{is}}$ for each layer and

Table 2. Mean values of pressure (in dbar), potential temperature (θ, in °C), salinity, apparent oxygen utilisation (AOU, in µmol kg^{-1}), total alkalinity (A_T, in µmol kg^{-1}), anthropogenic CO_2 (C_{ant}, in µmol kg^{-1}) and pH at total scale and in situ conditions of temperature and pressure ($pH_{T_{is}}$) for the bottom waters of the Iberian Abyssal Plain sampled during the seven OVIDE cruises. "N" represents the number of data considered in each cruise and "±" the standard deviation. The last row represents the intercruise standard deviation of the mean values.

Year (N)	Pressure	θ	Salinity	AOU	A_T	C_{ant}	$pH_{T_{is}}$
2002 (144)	4205	2.182 ± 0.080	34.913 ± 0.008	86.1 ± 2.0	2351 ± 3	6.4 ± 1.3	8.013 ± 0.003
2004 (158)	4263	2.162 ± 0.075	34.908 ± 0.007	87.1 ± 1.4	2352 ± 3	6.2 ± 1.2	8.013 ± 0.003
2006 (132)	4252	2.170 ± 0.082	34.913 ± 0.008	85.4 ± 1.6	2350 ± 3	6.2 ± 1.3	8.014 ± 0.003
2008 (125)	4206	2.179 ± 0.075	34.911 ± 0.007	84.9 ± 1.8	2353 ± 4	7.0 ± 1.6	8.016 ± 0.003
2010 (131)	4312	2.163 ± 0.077	34.908 ± 0.008	85.9 ± 1.6	2351 ± 3	7.0 ± 1.2	8.013 ± 0.002
2012 (102)	4397	2.149 ± 0.077	34.909 ± 0.008	87.9 ± 1.6	2352 ± 3	5.1 ± 1.2	8.015 ± 0.002
2014 (54)	4441	2.141 ± 0.069	34.904 ± 0.007	87.4 ± 1.36	2353 ± 3	5.5 ± 1.5	8.016 ± 0.003
		0.015	0.003	1.1	1.1	0.7	0.0015

year using the layer average value of "var" for each year but keeping the values of the other drivers constant and equal to the time-average value for the layer over the studied time period. Given that the variability of the physicochemical properties within each layer is relatively low (see standard deviations of the averaged values in Table S1), we can assume that these derivatives are constant over the studied time period and use a constant derivative value for each layer. Note that the sensitivity of $pH_{T_{is}}$ to changes in C_{ant} is the same as the sensitivity to changes in C_{nat} since both are DIC; therefore only $\frac{\partial pH_{T_{is}}}{\partial DIC}$ is necessary. To estimate each $\frac{dvar}{dt}$ term we performed a linear regression between var and time for each layer.

Due to the small range of pH change with which we are working and the relatively low pH variability within each layer, we can consider that pH follows a linear scale instead of a logarithmic scale. As a consequence the contributions of each of the terms considered in Eq. (2) to pH change are equivalent to the contributions in terms of $[H^+]$.

Trends of all variables involved in Eq. (2) were calculated based on the annual interpolation of the observed values to avoid the bias due to the reduced availability of cruises during the 1990s compared to the 2000s.

3 Results and discussion

3.1 Distribution of water mass properties

The Irminger and Iceland basins in the North Atlantic are characterised by warm and saline surface waters as well as cold and less saline intermediate and deep waters (Fig. 2a, b). The central waters (here represented by the SPMW layer), which dominates the upper ~ 700 m, are warmer and saltier in the Iceland basin than in the Irminger basin, reflecting the water mass transformation that takes place along the path of the North Atlantic Current (NAC) (Brambilla and Talley, 2008). In particular, the mixing of the SPMW layer with the surrounding waters while flowing around the Reykjanes Ridge (evident in the salinity distribution; see also García-Ibáñez et al., 2015), in conjunction with the air–sea heat loss, results in a colder and fresher SPMW layer in the Irminger basin. The uLSW and cLSW layers below the SPMW layer are saltier in the Iceland basin due to their mixing with the surrounding waters during their journey from their formation regions (Bersch et al., 1999; Pickart et al., 2003; García-Ibáñez et al., 2015). The ISOW layer dominates at depths beneath the cLSW layer. This layer is saltier in the Iceland basin, reflecting its circulation. ISOW comes from the Iceland–Scotland sill and flows southwards into the Iceland basin, where it mixes with the older North Atlantic Deep Water (NADW). Then it crosses the Reykjanes Ridge through the Charlie–Gibbs Fracture Zone (Fig. 1a), where it mixes with the cLSW and DSOW, becoming fresher. At the bottom of the Irminger basin a fifth layer, DSOW, being the coldest and freshest layer of the section, is distinguished.

The general pattern of $pH_{T_{is}}$ (Fig. 2c) by and large follows the distribution expected from the surface production of organic material and remineralisation at depth. Consequently, high pH values (> 8.05) are found in upper layers, while the values generally decrease with depth down to < 7.95 in the deepest layers. This overall pattern is disrupted at ~ 500 m in the Iceland basin by a layer with relatively low $pH_{T_{is}}$ values (< 7.98), coinciding with relatively high AOU and DIC values (Fig. 2e, f). This layer could be associated with an area of slower circulation where the products of the remineralisation of the organic matter accumulate. This thermocline layer could also be influenced by waters of southern origin (Sarafanov et al., 2008) which are advected into the region by the NAC, which has an extension that is closely related to the North Atlantic Oscillation (Desbruyères et al., 2013). The presence of this low pH layer lowers the average pH of our SPMW layer in the Iceland basin compared to the Irminger basin (Fig. 3). The opposite pattern is found in the uLSW layer. The water mass formation occurring in the Irminger basin (Pickart et al., 2003; García-Ibáñez et al., 2015; Fröb et al., 2016; Piron et al., 2016) transfers recently ventilated low DIC and high pH waters to depth, which causes the mean

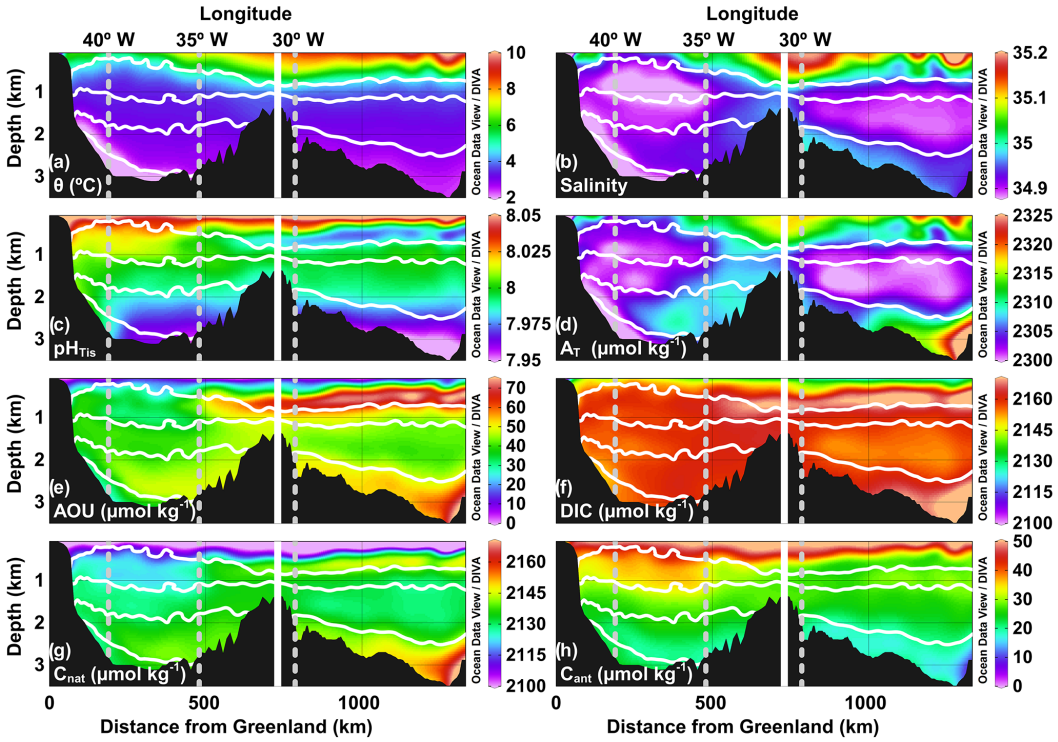

Figure 2. Distributions along the cruise track from Greenland (left) to the Iceland basin (right) over the study period (1991–2015) for **(a)** potential temperature (θ, in °C), **(b)** salinity, **(c)** pH at total scale and in situ conditions (pH$_{T_{is}}$), **(d)** total alkalinity (A_T, in µmol kg^{-1}), **(e)** apparent oxygen utilisation (AOU, in µmol kg^{-1}), **(f)** total dissolved inorganic carbon (DIC; in µmol kg^{-1}), **(g)** natural DIC (C_{nat}, in µmol kg^{-1}) and **(h)** anthropogenic CO_2 (C_{ant}, in µmol kg^{-1}) for the 2004 cruise. The dashed vertical lines represent the longitude axis marks, and isopycnals delineating the layers are shown as white lines.

pH of uLSW in the Irminger basin to be higher than in the Iceland basin. Finally, the layers that contain the overflow waters have the lowest pH values. The presence of the older NADW in the ISOW layer in the Iceland basin decreases the mean pH of this layer here, making it lower than in the Irminger basin.

The upper layer waters of the section have low DIC values, which rapidly increase when increasing depth (Fig. 2f). The low DIC values in the uppermost ∼ 200 m are a consequence of the photosynthetic activity that withdraws DIC from seawater. Below ∼ 200 m the DIC distribution is almost homogeneous, only disrupted by relatively high values in the Iceland basin at ∼ 500 m, associated with the thermocline layer, and at the bottom, associated with the old NADW. The gradients in anthropogenic and natural components of DIC are much stronger. The C_{ant} values are high, close to saturation (approximately 80 % of the C_{ant} concentration expected from a surface ocean in equilibrium with the atmospheric CO_2), near the surface and decrease with depth (Fig. 2h), because C_{ant} enters the ocean from the atmosphere. The C_{nat} distribution has an opposite pattern, with low surface values and high bottom values (Fig. 2g), similar to that of the AOU distribution (Fig. 2e), since C_{nat} is linked to the ventilation of water masses, i.e. respiration and renewal of the water mass.

The A_T distribution along the section resembles the salinity distribution, with high values associated with the relatively saline central waters and relatively low and almost homogeneous values in the rest of the section (Fig. 2d). The exception comes with the ISOW layer. The high A_T values found in the ISOW layer of the Iceland basin are not mirrored in the salinity distribution. This reflects the influence of NADW that is traced by the relatively large amounts of silicate related to the influence of the Antarctic Bottom Water, which provides high A_T from dissolution of $CaCO_3$. The influence of these high A_T values is then transported by the ISOW circulation to the Irminger basin.

3.2 Water mass acidification and drivers

Trends of pH$_{T_{is}}$ in each layer and basin are presented in Table 3, in Fig. 3 and in Supplement Fig. S1. The pH$_{T_{is}}$ has decreased in all layers of the Irminger and Iceland basins during a time period of more than 20 years (1991–2015) that is covered by the data. The trends are stronger in the Irminger basin due to the presence of younger waters. The rate of pH decline decreases with depth, except for the DSOW layer that has acidification rates close to those found in the cLSW layer. This indicates that DSOW is a newly formed water mass that

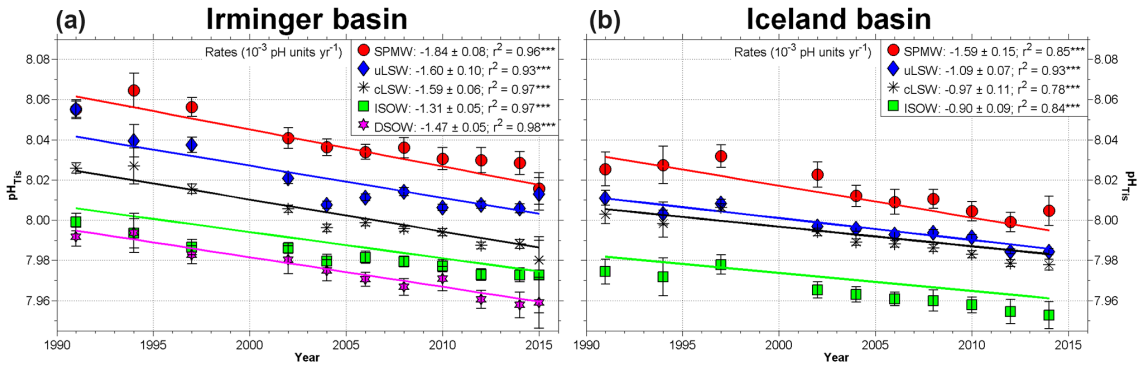

Figure 3. Temporal evolution of average pH at total scale and in situ conditions of temperature and pressure ($pH_{T_{is}}$) in the main water masses of the Irminger **(a)** and Iceland **(b)** basins between 1991 and 2015. Each point represents the average $pH_{T_{is}}$ of a particular layer (SPMW (red dots), uLSW (blue diamonds), cLSW (black asterisks), ISOW (green squares) and DSOW (magenta stars)) at the time of each cruise (Table S1). The error bars are two times the error of the mean ($2\sigma = 2\times$(Standard Deviation)$/\sqrt{N}$, where "N" is the number of samples of each layer). The legends also give the trends (in 10^{-3} pH units yr^{-1}) ± standard error of the estimate and the correlation coefficients (r^2), resulting from the annually interpolated values. *** denotes that the trend is statistically significant at the 99 % level (p value < 0.01). Consult Fig. 1 for layer acronyms.

has recently been in contact with the atmosphere. Moreover, the acidification rate in the ISOW layer in the Irminger basin is relatively low, which could be related to the increasing importance of the relatively old NADW in this layer, with the reduction in cLSW formation since the mid-90s (Lazier et al., 2002; Yashayaev, 2007).

The observed rate of $pH_{T_{is}}$ decrease in the SPMW layer of the Iceland basin (-0.0016 ± 0.0001 pH units yr^{-1}; Table 3, Fig. 3b) is in agreement with that observed at the Iceland Sea time series (68° N, 12.66° W; Olafsson et al., 2009, 2010) for the period 1983–2014 (-0.0014 ± 0.0005 pH units yr^{-1}; Bates et al., 2014). However, our rate of $pH_{T_{is}}$ decrease in the SPMW layer in the Irminger basin (-0.0018 ± 0.0001 pH units yr^{-1}) is lower than that observed in the sea surface waters of the Irminger Sea time series (64.3° N, 28° W; Olafsson et al., 2010) for the period 1983–2014 (-0.0026 ± 0.0006 pH units yr^{-1}; Bates et al., 2014), which is exceptionally high compared to the other time series summarised here. Bates et al. (2014) linked the high acidification rate found at the Irminger Sea time series to the high rate of increase in DIC (1.62 ± 0.35 µmol kg^{-1} yr^{-1}) observed at this site, which is almost three times our rate of increase in DIC (0.64 ± 0.07 µmol kg^{-1} yr^{-1}, Fig. 5c). This is based on data from only one site, further north than our section, and indicates that spatial variations are substantial in this region. Besides, the acidification rates in the SPMW layer of both basins reported here are in agreement with the rates of -0.0020 ± 0.0004 pH units yr^{-1} determined for the North Atlantic subpolar seasonally stratified biome for the period 1991–2011 (Lauvset et al., 2015). Compared to the subtropical Atlantic time series stations, our rates in the SPMW layer of both basins are in agreement with those observed at ESTOC (European Station for Time series in the ocean) (29.04° N, 15.50° W; Santana-Casiano et al., 2007; González-Dávila et al., 2010) for the period 1995–2014 (-0.0018 ± 0.0002 pH units yr^{-1}; Bates et al., 2014) and BATS (Bermuda Atlantic Time-series Study) (32° N, 64° W; Bates et al., 2014) for the period 1983–2014 (-0.0017 ± 0.0001 pH units yr^{-1}; Bates et al., 2014). Compared to the Pacific Ocean, the OA rates in the Iceland and Irminger basins are in agreement with those reported for the central North Pacific based on data from the time series station HOT (Hawaii Ocean Time-series) (22.45° N, 158° W; Dore et al., 2009) for the period 1988–2014 (-0.0016 ± 0.0001 pH units yr^{-1}; Bates et al., 2014), but are slightly higher than those determined by Wakita et al. (2013) in the winter mixed layer at the subarctic western North Pacific (time series stations K2 and KNOT) for the period 1997–2011 (-0.0010 ± 0.0004 pH units yr^{-1}). Wakita et al. (2013) attributed the lower-than-expected pH trends to an increasing A_T trend.

To infer the causes of the acidification trends reported here, we decomposed the pH trends into their individual components as described in Sect. 2.2. The values of each term, $\frac{\partial pH_{T_{is}}}{\partial var}$ and $\frac{dvar}{dt}$ (where "var" refers to each of the drivers), described in Sect. 2.2 can be found in the Supplement in Table S2 and Figs. 4–6, respectively. The results of solving Eq. (2) are presented in Table 3. The sum of the pH changes caused by the individual drivers, i.e. $\left(\frac{dpH_{T_{is}}}{dt}\right)_{total}$ matches the observed pH trends $\left(\left(\frac{dpH_{T_{is}}}{dt}\right)_{obs}\right)$, which renders confidence to the method.

The temperature changes (Fig. 4a, b) have generally resulted in small-to-negligible pH declines (Table 3). Specifically, warming corresponds to a pH decrease of at least 0.0002 pH units yr^{-1} in the SPMW layer of the Iceland basin

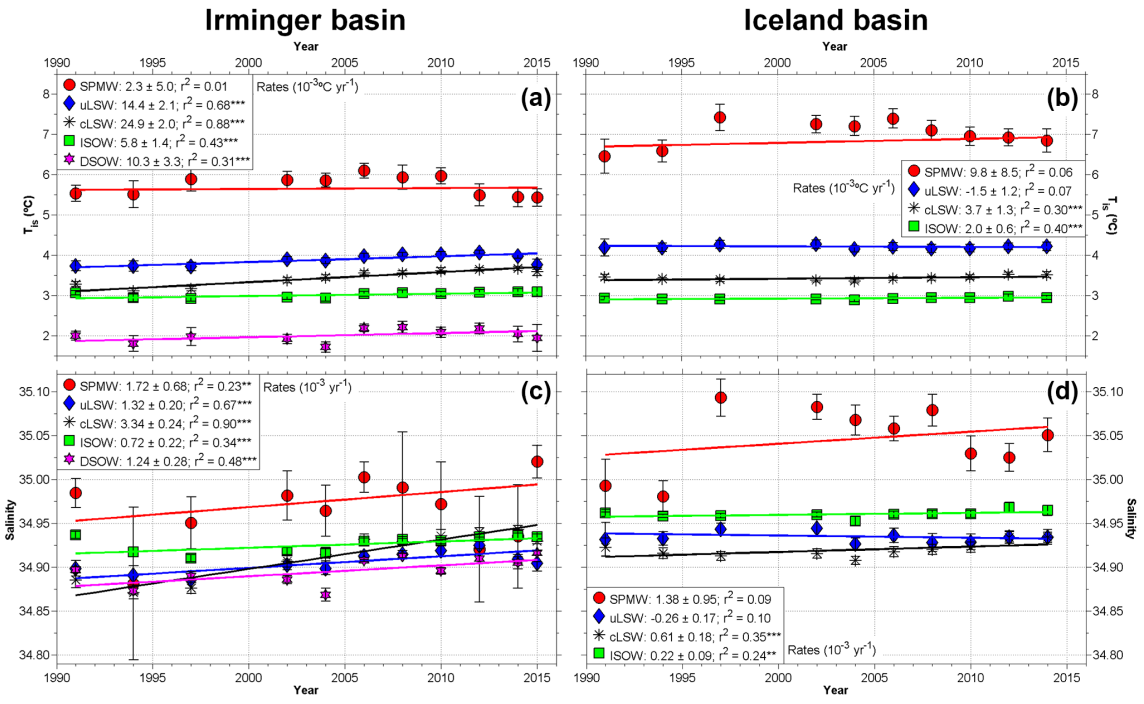

Figure 4. Temporal evolution between 1991 and 2015 of average **(a, b)** in situ temperature (T_{is}, in °C) and **(c, d)** salinity in the main water masses of the Irminger **(a, c)** and Iceland **(b, d)** basins. Each point represents the average property of a particular layer (SPMW (red dots), uLSW (blue diamonds), cLSW (black asterisks), ISOW (green squares) and DSOW (magenta stars)) at the time of each cruise (Table S1). The error bars are 2σ. The legends also give the trends (in 10^{-3} units yr^{-1}) ± standard error of the estimate and the correlation coefficients (r^2), resulting from the annually interpolated values. ** denotes that the trend is statistically significant at the 95 % level (p value < 0.05) and *** at the 99 % level (p value < 0.01). Consult Fig. 1 for layer acronyms.

and in the LSW and DSOW layers of the Irminger basin, while the effect of temperature changes on pH in the other layers is negligible. Temperature-driven pH change is larger in the LSW layers in the Irminger than in the Iceland basin. In the case of the uLSW layer, this is possibly explained by the deep convection occurring in the Irminger basin (Pickart et al., 2003; García-Ibáñez et al., 2015; Fröb et al., 2016; Piron et al., 2016). In the case of the cLSW layer, the higher pH changes driven by temperature changes in the Irminger basin could be explained by the rapid advection of the water mass from the Labrador Sea to this basin (Yashayaev et al., 2007). Temperature driven pH change in the DSOW layer could be related to the entrainment of LSW into DSOW that takes place downstream of the Greenland–Iceland sills (Read, 2000; Yashayaev and Dickson, 2008). The temperature effect on pH evaluated here is thermodynamic. The same applies to the salinity effect, which however is small to negligible, reflecting how salinity changes in the region (Fig. 4c, d) are insufficiently large to significantly change pH.

Overall, the A_T has increased in the Irminger and Iceland basins (Fig. 5a, b), corresponding to increasing pH (Table 3), which counteracts the acidification from the CO_2 absorption. The contribution from A_T to reduce ocean acidification is significant in all layers except for uLSW of the Iceland basin (where the trend in A_T is decreasing, but not significant; Fig. 5b). The similar behaviour of the salinity and A_T trends over time may indicate that the changes in A_T are mainly driven by changes in salinity. The A_T increasing trends observed in the SPMW layer could be related to the increasing presence of waters of subtropical origin (with higher A_T) as the subpolar gyre was shrinking from the mid-90s into the 2000s (e.g. Flatau et al., 2003; Häkkinen and Rhines, 2004; Böning et al., 2006). In the case of the LSW layers, the increase in A_T can be explained by the mid-90s cessation of the cLSW formation (Lazier et al., 2002; Yashayaev, 2007), with the consequent salinisation (and increase in A_T) of this water mass. The signal of the cLSW salinisation was then transmitted to the overflow layers due to the entrainment events (Sarafanov et al., 2010).

The DIC increase (Fig. 5c, d) is the main cause of the observed pH decreases (Table 3) and corresponds to pH drops between -0.00099 ± 0.00014 and -0.00205 ± 0.00011 pH units yr^{-1}. The waters in both the Irminger and Iceland basins gained DIC in response to the increase in atmospheric CO_2; the convection processes occurring in the former basin (Pickart et al., 2003; Thierry et al., 2008; de Boisséson et al., 2010; García-Ibáñez et al., 2015; Fröb et al., 2016; Piron et al., 2016) and in the sur-

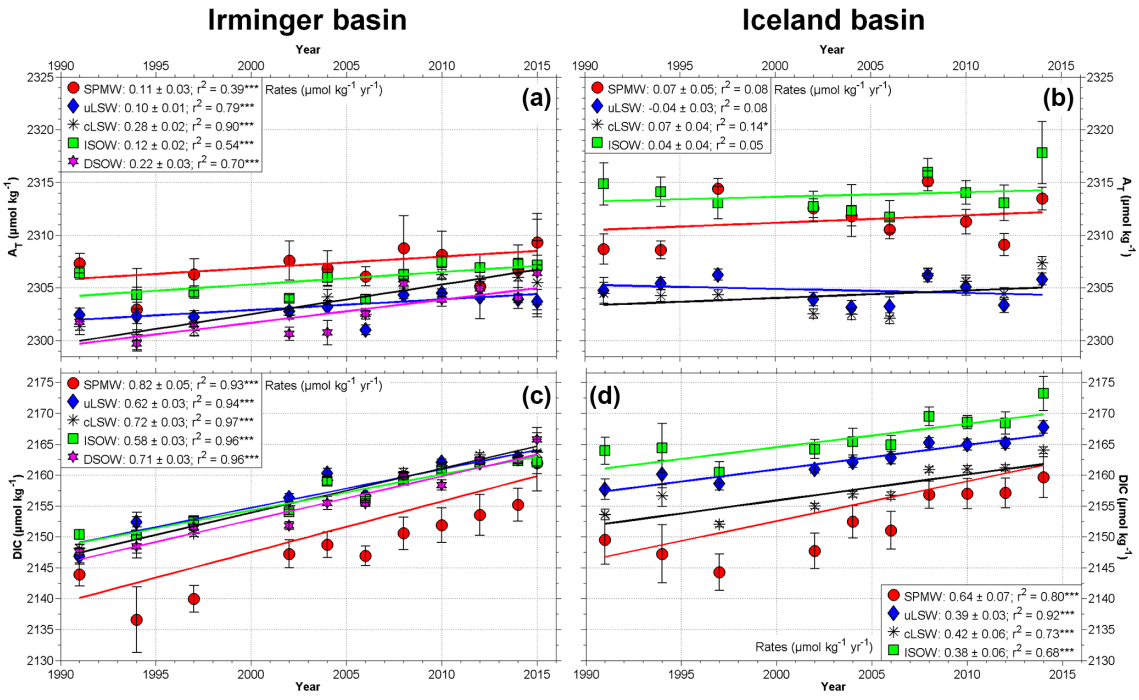

Figure 5. Temporal evolution between 1991 and 2015 of average **(a, b)** total alkalinity (A_T, in µmol kg^{-1}) and **(c, d)** total dissolved inorganic carbon (DIC, in µmol kg^{-1}) in the main water masses of the Irminger **(a, c)** and Iceland **(b, d)** basins. Each point represents the average property of a particular layer (SPMW (red dots), uLSW (blue diamonds), cLSW (black asterisks), ISOW (green squares) and DSOW (magenta stars)) at the time of each cruise (Table S1). The error bars are 2σ. The legends also give the trends (in µmol kg^{-1} yr^{-1}) ± standard error of the estimate and the correlation coefficients (r^2), resulting from the annually interpolated values. * denotes that the trend is statistically significant at the 90 % level (p value < 0.1) and *** at the 99 % level (p value < 0.01). Consult Fig. 1 for layer acronyms.

rounding ones (i.e. Labrador and Nordic seas) provide an important pathway for DIC to pass from the surface mixed layer to the intermediate and deep layers. The effect of the DIC increase on pH is generally dominated by the anthropogenic component (Table 3). The exception comes with the cLSW layer of the Irminger basin, where the natural component resulting from the aging of the layer dominates. In general, the Irminger basin layers have higher C_{ant} increase rates than the Iceland basin layers (Fig. 6a, b) and therefore larger pH declines, presumably a result of convection in the Irminger basin itself and advection of newly ventilated waters from the Labrador Sea. The highest C_{ant} increase rates are found in the SPMW layers, owing to their direct contact with the atmosphere, and result in the strongest rates of pH decrease. In the Irminger basin, the rise in C_{ant} levels of the SPMW layer correspond to about 87 % of the rate expected from a surface ocean maintaining its degree of saturation with the atmospheric CO_2 rise (computed using the globally averaged marine surface annual mean pCO_2 data from the NOAA as a reference, ftp://aftp.cmdl.noaa.gov/products/trends/co2/co2_annmean_gl.txt), while in the Iceland basin, this rate is about 73 % of the expected rate. The lower fraction in the Iceland basin compared to the Irminger basin is a consequence of the inclusion of the aforementioned poorly ventilated thermocline waters in our SPMW layer (Fig. 2e, h). Note than none of the C_{ant} trends of the SPMW layers correspond to 100 % of the rate expected from assuming saturation with the atmospheric CO_2 rise. This can be explained by the fact that surface water CO_2 concentration rise lags behind that of the atmosphere by between two and five years in this region (Biastoch et al., 2007; Jones et al., 2014). We also note that the temperature and A_T changes impact the pH of the SPMW layer, decreasing and increasing it, respectively. This could indicate that the increasing presence of warmer and more saline (with higher A_T) waters of subtropical origin partially counteracts the effects of increasing DIC values, because A_T effects dominate (as stated before, the effect of salinity change on pH is negligible). Overall this change can be explained as the result of the contraction of the subpolar gyre that took place since the mid-90s (e.g. Flatau et al., 2003; Häkkinen and Rhines, 2004; Böning et al., 2006). Wakita et al. (2013) also found lower-than-expected acidification rates in the surface waters of the Pacific Ocean, which they explained as being the consequence of increasing A_T. Finally, the strong influence of the anthropogenic component on the pH decrease of the DSOW layer stands out and is the main agent of the pH decline in this layer.

The pH changes related to C_{nat} changes (Fig. 6c, d) can be interpreted as changes related to ventilation of water masses and water mass changes (with different A_T and DIC).

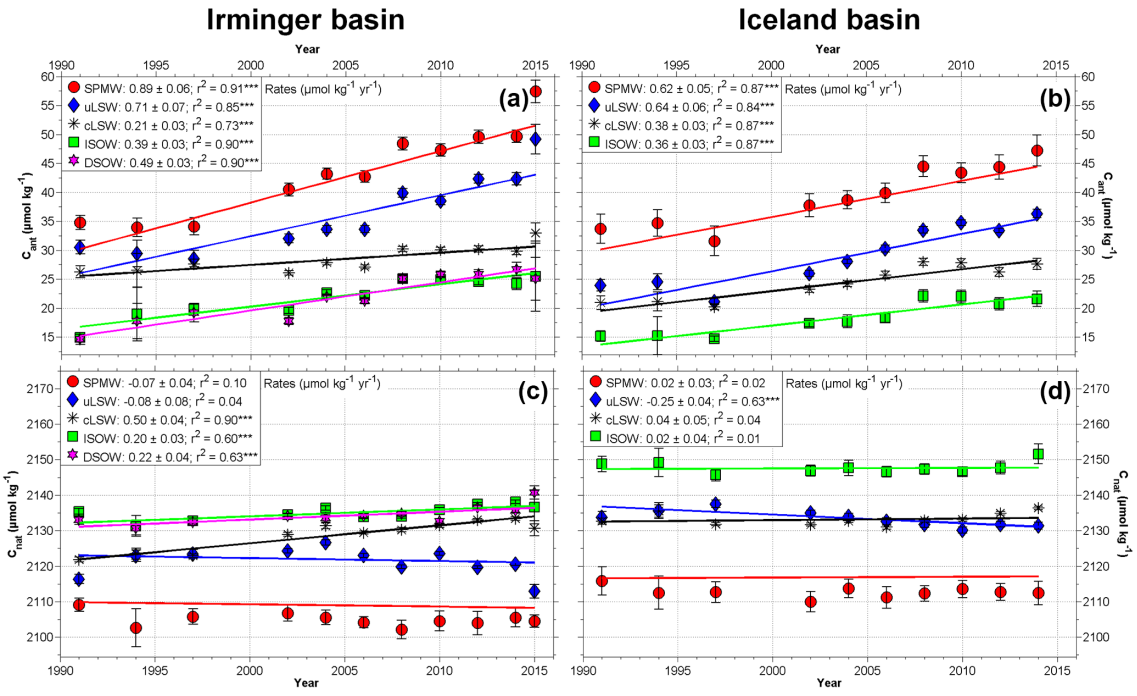

Figure 6. Temporal evolution between 1991 and 2015 of average **(a, b)** anthropogenic CO_2 (C_{ant}, in µmol kg^{-1}) and **(c, d)** natural DIC ($C_{nat} = DIC - C_{ant}$, in µmol kg^{-1}) values in the main water masses of the Irminger **(a, c)** and Iceland **(b, d)** basins. Each point represents the average property of a particular layer (SPMW (red dots), uLSW (blue diamonds), cLSW (black asterisks), ISOW (green squares) and DSOW (magenta stars)) at the time of each cruise (Table S1). The error bars are 2σ. The legends also give the trends (in µmol kg^{-1} yr^{-1}) ± standard error of the estimate and the correlation coefficients (r^2), resulting from the annually interpolated values. *** denotes that the trend is statistically significant at the 99 % level (p value < 0.01). Consult Fig. 1 for layer acronyms.

Stronger pH decreases related to C_{nat} changes indicate a lack of ventilation and accumulation of DIC from remineralised organic material. This is clearly the case for the cLSW layer, where the observed pH decrease is caused by a combination of the effects of C_{ant} and C_{nat} (Table 3). The greater influence of C_{nat} in the cLSW layer is the result of the ageing of this water mass after its last formation event in the mid-90s (e.g. Lazier et al., 2002; Azetsu-Scott et al., 2003; Kieke et al., 2007; Yashayaev, 2007). A similar effect of C_{nat} changes on pH is observed in the overflow layers of the Irminger basin, which are influenced by the mixing with cLSW (García-Ibáñez et al., 2015). Finally, there is a contrast between the C_{nat} influence on the pH of the uLSW layer in both basins. The interannual variability of the uLSW properties attenuates due to mixing over the length and timescales of the transit from the Labrador Sea (Cunningham and Haine, 1995; Paillet et al., 1998), which causes the interannual variability in the C_{nat} values of the uLSW layer in the Iceland basin to be smoother than in the Irminger basin (Fig. 6c, d). Therefore, the lower interannual variability in the C_{nat} values of the uLSW layer in the Iceland basin promotes better detectability of the ventilation of the uLSW layer, resulting in an offset up to 60 % of the effects of acidification on the uLSW layer of the Iceland basin.

Vázquez-Rodríguez et al. (2012b) previously studied the pH changes in the different water masses of the Irminger and Iceland basins. These authors carried out a pH normalisation to avoid potential biases due to different ventilation stages and rates of each layer from the different spatial coverage of the evaluated cruises. The normalised pH values (pH_N) for each layer were obtained using multiple linear regressions between the observed mean pH_{SWS25} (pH at seawater scale and 25 °C) and the observed mean values of θ, salinity, silicate and AOU, referring to the mean climatological values of θ, salinity, silicate and AOU compiled in WOA05 (http://www.nodc.noaa.gov/OC5/WOA05/pr_woa05.html). This normalisation, combined with the different temporal coverage (1981–2008), causes the rates reported by Vázquez-Rodríguez et al. (2012b) to differ from those obtained in the present work. The pH_N trends reported for the SPMW and uLSW layers of the Irminger basin and for the ISOW layer of the Iceland basin are very similar to our $pH_{T_{is}}$ trends for these layers. However, the pH_N trends reported by Vázquez-Rodríguez et al. (2012b) for the cLSW layer in both basins and for the ISOW layer in the Irminger basin are significantly different from our $pH_{T_{is}}$ trends for these layers, but are very similar to pH changes derived from C_{ant} changes: $\frac{\partial pH_{T_{is}}}{\partial DIC}\frac{dC_{ant}}{dt}$ (Table 3). In the case of the DSOW

Table 3. Observed temporal changes of pH at total scale and in situ temperature and pressure conditions: $\left(\frac{\mathrm{dpH_{T_{is}}}}{\mathrm{d}t}\right)_{\mathrm{obs}}$ for the main water masses in the Irminger and Iceland basins for the period 1991–2015. pH changes caused by the main drivers (in situ temperature, T_{is}; salinity, S; total alkalinity, A_T; total dissolved inorganic carbon, DIC; the latter decomposed into its anthropogenic and natural components, C_{ant} and C_{nat}, respectively) are also shown, as well as the pH changes determined as the sum of the pH changes caused by the individual drivers $\left(\left(\frac{\mathrm{dpH_{T_{is}}}}{\mathrm{d}t}\right)_{\mathrm{total}}\right)$. All the trends are calculated based on the annually interpolated values and are in 10^{-3} pH units yr^{-1}. Values in parenthesis are the percentages of the observed pH change explained by each one of its drivers. Consult Fig. 1 for water mass acronyms.

		$\left(\frac{\mathrm{dpH_{T_{is}}}}{\mathrm{d}t}\right)_{\mathrm{obs}}$	$\frac{\partial \mathrm{pH_{T_{is}}}}{\partial T_{is}}\frac{\mathrm{dT_{is}}}{\mathrm{d}t}$	$\frac{\partial \mathrm{pH_{T_{is}}}}{\partial S}\frac{\mathrm{dS}}{\mathrm{d}t}$	$\frac{\partial \mathrm{pH_{T_{is}}}}{\partial A_T}\frac{\mathrm{dA_T}}{\mathrm{d}t}$	$\frac{\partial \mathrm{pH_{T_{is}}}}{\partial \mathrm{DIC}}\frac{\mathrm{dDIC}}{\mathrm{d}t}$	$\frac{\partial \mathrm{pH_{T_{is}}}}{\partial \mathrm{DIC}}\frac{\mathrm{dC_{ant}}}{\mathrm{d}t}$	$\frac{\partial \mathrm{pH_{T_{is}}}}{\partial \mathrm{DIC}}\frac{\mathrm{dC_{nat}}}{\mathrm{d}t}$	$\left(\frac{\mathrm{dpH_{T_{is}}}}{\mathrm{d}t}\right)_{\mathrm{total}}$
Irminger	SPMW	−1.84 ± 0.08	−0.04 ± 0.08 (2)	−0.021 ± 0.008 (1)	0.26 ± 0.07 (−14)	−2.05 ± 0.11 (111)	−2.21 ± 0.14 (120)	0.16 ± 0.10 (−9)	−1.85 ± 0.15 (100.5)
	uLSW	−1.60 ± 0.10	−0.23 ± 0.03 (14)	−0.016 ± 0.002 (1)	0.25 ± 0.03 (−16)	−1.61 ± 0.08 (101)	−1.83 ± 0.16 (114)	0.22 ± 0.21 (−14)	−1.61 ± 0.09 (100.6)
	cLSW	−1.59 ± 0.06	−0.40 ± 0.03 (25)	−0.040 ± 0.003 (3)	0.70 ± 0.05 (−44)	−1.85 ± 0.07 (116)	−0.55 ± 0.07 (34)	−1.31 ± 0.09 (82)	−1.60 ± 0.09 (100.3)
	ISOW	−1.31 ± 0.05	−0.09 ± 0.02 (7)	−0.009 ± 0.003 (1)	0.29 ± 0.06 (−22)	−1.50 ± 0.07 (115)	−0.99 ± 0.07 (76)	−0.50 ± 0.09 (39)	−1.31 ± 0.09 (100.1)
	DSOW	−1.47 ± 0.05	−0.16 ± 0.05 (11)	−0.015 ± 0.003 (1)	0.55 ± 0.07 (−37)	−1.85 ± 0.08 (126)	−1.27 ± 0.09 (87)	−0.58 ± 0.09 (39)	−1.48 ± 0.12 (100.6)
Iceland	SPMW	−1.59 ± 0.15	−0.16 ± 0.13 (10)	−0.016 ± 0.011 (1)	0.17 ± 0.12 (−11)	−1.60 ± 0.17 (101)	−1.54 ± 0.13 (97)	−0.06 ± 0.08 (4)	−1.60 ± 0.24 (100.9)
	uLSW	−1.09 ± 0.07	0.02 ± 0.02 (−2)	0.003 ± 0.002 (0)	−0.10 ± 0.07 (9)	−1.03 ± 0.06 (95)	−1.68 ± 0.15 (154)	0.65 ± 0.11 (−60)	−1.10 ± 0.10 (101.0)
	cLSW	−0.97 ± 0.11	−0.06 ± 0.02 (6)	−0.007 ± 0.002 (1)	0.18 ± 0.09 (−18)	−1.09 ± 0.14 (112)	−0.98 ± 0.08 (100)	−0.12 ± 0.11 (12)	−0.98 ± 0.17 (101.0)
	ISOW	−0.90 ± 0.09	−0.03 ± 0.01 (4)	−0.003 ± 0.001 (0)	0.11 ± 0.10 (−12)	−0.99 ± 0.14 (110)	−0.95 ± 0.08 (105)	−0.04 ± 0.11 (5)	−0.91 ± 0.18 (101.6)

layer, the $\mathrm{pH_N}$ trend is also in agreement with $\frac{\partial \mathrm{pH_{T_{is}}}}{\partial \mathrm{DIC}}\frac{\mathrm{d}C_{ant}}{\mathrm{d}t}$ trends. This suggests that the normalisation carried out by Vázquez-Rodríguez et al. (2012b) could remove some of the impact of the natural component (represented here by C_{nat}) over pH changes, essentially due to the use of AOU in the normalisation.

4 Conclusions

The progressive acidification of the North Atlantic waters has been assessed from direct observations obtained over the last 25 years (1991–2015), with the greatest pH decreases observed in surface and intermediate waters. From the study of the main drivers of the observed pH changes we conclude that the observed pH decreases are mainly a consequence of the oceanic C_{ant} uptake. In addition we find that they have been partially offset by A_T increases. Thus, while the C_{ant} concentration of the upper layer roughly keeps up with the concentration expected from rising atmospheric CO_2, the pH decreases at a lower rate than expected from C_{ant} increase. The increasing arrival of saline and alkaline subtropical waters transported by the NAC to the study region, related to the contraction of the subpolar gyre since the mid-90s, buffers the acidification caused by the C_{ant} increase in the upper layer. The acidification rates in intermediate waters are similar to those in the surface waters and are caused by a combination of anthropogenic and non-anthropogenic components. The acidification of cLSW due to the C_{ant} uptake is reinforced by the aging of this water mass from the end of the 1990s onwards. The pH of the deep waters of the Irminger basin, DSOW, has clearly decreased in response to anthropogenic forcing. We also infer that water mass warming contributes between 2 and 25 % to the pH decrease of the upper and intermediate waters of the Irminger basin, and 10 % to the pH decrease of the upper waters of the Iceland basin.

5 Data availability

OVIDE 2012 data was accessed from the Clivar & Carbon Hydrographic Data Office (CCHDO; http://cchdo.ucsd.edu/cruise/29AH20120622), and OVIDE 2014 data is publicly available at http://www.obs-vlfr.fr/proof/ftpfree/geovide/ALKALINITY_PH/. The data from the 58GS20150410 cruise is unpublished and can be obtained per request to Are Olsen (are.olsen@gfi.uib.no). They have not yet been made public in order to protect the interest of a PhD student who relies heavily on them for her work. It is our intention to release them when that has been completed, in 2017.

The Supplement related to this article is available online at doi:10.5194/bg-13-3701-2016-supplement.

Author contributions. All authors contributed extensively to the work presented in this paper. Maribel I. García-Ibáñez, Aida F. Ríos, Herlé Mercier, Are Olsen and Fiz F. Pérez designed the research. Maribel I. García-Ibáñez, Patricia Zunino, Friederike Fröb, Lidia I. Carracedo, Aida F. Ríos, Herlé Mercier, Are Olsen and Fiz F. Pérez analysed the physical and chemical data. Maribel I. García-Ibáñez and Patricia Zunino developed the code for processing the data. Maribel I. García-Ibáñez and Fiz F. Pérez determined the anthropogenic CO_2 concentrations, average layer properties and rates, and estimated the uncertainties. Maribel I. García-Ibáñez wrote the manuscript and prepared all figures, with contributions from all co-authors.

Acknowledgements. We are grateful to the captains, staff and researchers who contributed to the acquisition and processing of hydrographic data. The research leading to these results was supported through the EU FP7 project CARBOCHANGE "Changes in carbon uptake and emissions by oceans in a changing climate", which received funding from the European Commission's Seventh Framework Programme under grant agreement no. 264879. For this work M. I. Garcia-Ibáñez, A. F. Rios and F. F. Pérez were supported by the Spanish Ministry of Economy and Competitiveness through the BOCATS (CTM2013-41048-P) project co-funded by the Fondo Europeo de Desarrollo Regional 2007–2012 (FEDER). P. Zunino was supported by the GEOVIDE project as well as by IFREMER. L. I. Carracedo was funded by the University of Vigo, through the Galician I2C Plan for postdoctoral research. H. Mercier was supported by the French National Centre for Scientific Research (CNRS). F. Fröb and A. Olsen were supported by a grant from the Norwegian Research Council (SNACS, project 229756/E10).

Edited by: J. Middelburg

References

Anderson, L. G. and Olsen, A.: Air–sea flux of anthropogenic carbon dioxide in the North Atlantic, Geophys. Res. Lett., 29, 1835, doi:10.1029/2002GL014820, 2002.

Azetsu-Scott, K., Jones, E. P., Yashayaev, I., and Gershey, R. M.: Time series study of CFC concentrations in the Labrador Sea during deep and shallow convection regimes (1991–2000), J. Geophys. Res., 108, 3354, doi:10.1029/2002JC001317, 2003.

Bates, N., Astor, Y., Church, M., Currie, K., Dore, J., González-Dávila, M., Lorenzoni, L., Muller-Karger, F., Olafsson, J., and Santa-Casiano, M.: A Time-Series View of Changing Ocean Chemistry Due to Ocean Uptake of Anthropogenic CO_2 and Ocean Acidification, Oceanography, 27, 126–141, doi:10.5670/oceanog.2014.16, 2014.

Bates, N. R., Best, M. H. P., Neely, K., Garley, R., Dickson, A. G., and Johnson, R. J.: Detecting anthropogenic carbon dioxide uptake and ocean acidification in the North Atlantic Ocean, Biogeosciences, 9, 2509–2522, doi:10.5194/bg-9-2509-2012, 2012.

Benson, B. B. and Krause, D.: The concentration and isotopic fractionation of oxygen dissolved in freshwater and seawater in equilibrium with the atmosphere, Limnol. Oceanogr., 29, 620–632, doi:10.4319/lo.1984.29.3.0620, 1984.

Bersch, M., Meincke, J., and Sy, A.: Interannual thermohaline changes in the northern North Atlantic 1991–1996, Deep-Sea Res. Pt. II, 46, 55–75, doi:10.1016/S0967-0645(98)00114-3, 1999.

Biastoch, A., Völker, C., and Böning, C. W.: Uptake and spreading of anthropogenic trace gases in an eddy-permitting model of the Atlantic Ocean, J. Geophys. Res., 112, C09017, doi:10.1029/2006JC003966, 2007.

Böning, C. W., Scheinert, M., Dengg, J., Biastoch, A., and Funk, A.: Decadal variability of subpolar gyre transport and its reverberation in the North Atlantic overturning, Geophys. Res. Lett., 33, L21S01, doi:10.1029/2006GL026906, 2006.

Brambilla, E. and Talley, L. D.: Subpolar Mode Water in the northeastern Atlantic: 1. Averaged properties and mean circulation, J. Geophys. Res., 113, C04025, doi:10.1029/2006JC004062, 2008.

Broecker, W. S.: "NO" a conservative water mass tracer, Earth Planet. Sc. Lett., 23, 8761–8776, doi:10.1016/0012-821X(74)90036-3, 1974.

Caldeira, K. and Wickett, M.E.: Oceanography: Anthropogenic carbon and ocean pH, Nature, 425, 365–365, doi:10.1038/425365a, 2003.

Caldeira, K. and Wickett, M. E.: Ocean model predictions of chemistry changes from carbon dioxide emissions to the atmosphere and ocean, J. Geophys. Res., 110, C09S04, doi:10.1029/2004JC002671, 2005.

Carter, B. R., Radich, J. A., Doyle, H. L., and Dickson, A. G.: An automated system for spectrophotometric seawater pH measurements, Limnol. Oceanogr.-Meth., 11, 16–27, doi:10.4319/lom.2013.11.16, 2013.

Ciais, P., Sabine, C., Bala, G., Bopp, L., Brovkin, V., Canadell, J., Chhabra, A., DeFries, R., Galloway, J., Heimann, M., Jones, C., Le Quéré, C., Myneni, R. B., Piao, S., and Thornton, P.: Carbon and other biogeochemical cycles, in: Climate Change 2013: The Physical Science Basis. Contribution of Working Group I to the Fifth Assessment Report of the Intergovernmental Panel on Climate Change, edited by: Stocker, T. F., Qin, D., Plattner, G.-K., Tignor, M., Allen, S. K., Boschung, J., Nauels, A., Xia, Y., Bex, V., and Midgley, P. M., Cambridge University Press, Cambridge, United Kingdom and New York, NY, USA, 465–570, 2013.

Clayton, T. D. and Byrne, R. H.: Spectrophotometric seawater pH measurements: total hydrogen ion concentration scale calibration of m-cresol purple and at-sea results, Deep-Sea Res. Pt. I, 40, 2115–2129, doi:10.1016/0967-0637(93)90048-8, 1993.

Cunningham, S. A. and Haine, T. W. N.: Labrador Sea Water in the eastern North Atlantic. Part II: mixing dynamics and the advective-diffusive balance, J. Phys. Oceanogr., 14, 103–127, doi:10.1175/1520-0485(1995)025<0666:LSWITE>2.0.CO;2, 1995.

de Boisséson, E., Thierry, V., Mercier, H., and Caniaux, G.: Mixed layer heat budget in the Iceland Basin from Argo, J. Geophys. Res.-Oceans, 115, C10055, doi:10.1029/2010JC006283, 2010.

Desbruyères, D., Thierry, V., and Mercier, H.: Simulated decadal variability of the meridional overturning circulation across the A25-Ovide section, J. Geophys. Res.-Oceans, 118, 462–475, doi:10.1029/2012JC008342, 2013.

DeVries, T.: The oceanic anthropogenic CO_2 sink: Storage, air-sea fluxes, and transports over the industrial era, Global Biogeochem. Cy., 28, 631–647, doi:10.1002/2013GB004739, 2014.

Dickson, A. and Goyet, C.: Handbook of methods for the analysis of the various parameters of the carbon dioxide system in sea water, Version 2, Oak Ridge National Laboratory, Oak Ridge, TN, doi:10.2172/10107773, 198 pp., 1994.

Dickson, A. and Millero, F.: A comparison of the equilibrium constants for the dissociation of carbonic acid in seawater media, Deep-Sea Res., 34, 1733–1743, doi:10.1016/0198-0149(87)90021-5, 1987.

Dickson, A. G., Sabine, C. L., and Christian, J. R.: Guide to best practices for ocean CO_2 measurements, PICES Spec. Publ., 3, North Pacific Marine Science Organization Sidney, British Columbia, 191 pp., 2007.

Doney, S. C., Fabry, V. J., Feely, R. A., and Kleypas, J. A.: Ocean acidification: the other CO_2 problem, Annu. Rev. Mar. Sci., 1, 169–192, doi:10.1146/annurev.marine.010908.163834, 2009.

Dore, J. E., Lukas, R., Sadler, D. W., Church, M. J., and Karl, D. M.: Physical and biogeochemical modulation of ocean acidification in the central North Pacific, P. Natl. Acad. Sci. USA, 106, 12235–12240, doi:10.1073/pnas.0906044106, 2009.

Eakins, B. W. and Sharman, G. F.: Volumes of the World's Oceans from ETOPO1, NOAA National Geophysical Data Center, Boulder, CO, 2010.

Feely, R. A., Sabine, C. L., Lee, K., Berelson, W., Kleypas, J., Fabry, V. J., and Millero, F. J.: Impact of Anthropogenic CO_2 on the $CaCO_3$ System in the Oceans, Science, 305, 362–366, doi:10.1126/science.1097329, 2004.

Feely, R. A., Doney, S. C., and Cooley, S. R.: Ocean acidification: Present and future changes in a high-CO_2 world, Oceanography, 22, 36–47, doi:10.5670/oceanog.2009.95, 2009.

Flatau, M. K., Talley, L., and Niiler, P. P.: The North Atlantic Oscillation, Surface Current Velocities, and SST Changes in the Subpolar North Atlantic, J. Clim., 16, 2355–2369, doi:10.1175/2787.1, 2003.

Fröb, F., Olsen, A., Våge, K., Moore, K., Yashayaev, I., Jeannson, E., and Rajasakaren, B.: Record deep convection in the Irminger Sea in winter 2014-15, OSM, New Orleans, Louisiana, USA, 21–16 February 2016, HE11A-02, 2016.

García-Ibáñez, M. I., Pardo, P. C., Carracedo, L. I., Mercier, H., Lherminier, P., Ríos, A. F., and Pérez, F. F.: Structure, transports and transformations of the water masses in the Atlantic Subpolar Gyre, Prog. Oceanogr., 135, 18–36, doi:10.1016/j.pocean.2015.03.009, 2015.

Gehlen, M., Gruber, N., Gangstø, R., Bopp, L., and Oschlies, A.: Biogeochemical consequences of ocean acidification and feedbacks to the earth system, in: Ocean Acidification, Vol. 1, edited by: Gattuso, J.-P. and Hansson, L., Oxford University Press, 230–248, 2011.

González-Dávila, M., Santana-Casiano, J. M., Rueda, M. J., and Llinás, O.: The water column distribution of carbonate system variables at the ESTOC site from 1995 to 2004, Biogeosciences, 7, 3067—3081, doi:10.5194/bg-7-3067-2010, 2010.

Gourcuff, C., Lherminier, P., Mercier, H., and Le Traon, P. Y.: Altimetry Combined with Hydrography for Ocean Transport Estimation, J. Atmos. Ocean. Tech., 28, 1324–1337, doi:10.1175/2011JTECHO818.1, 2011.

Gruber, N., Sarmiento, J. L., and Stocker, T. F.: An improved method for detecting anthropogenic CO_2 in the oceans, Global Biogeochem. Cy., 10, 809–837, doi:10.1029/96GB01608, 1996.

Guallart, E. F., Fajar, N. M., Padín, X. A., Vázquez-Rodríguez, M., Calvo, E., Ríos, A. F., Hernández-Guerra, A., Pelejero, C., and Pérez, F. F.: Ocean acidification along the 24.5° N section in the subtropical North Atlantic, Geophys. Res. Lett., 42, 450–458, doi:10.1002/2014GL062971, 2015.

Häkkinen, S. and Rhines, P. B.: Decline of subpolar North Atlantic circulation during the 1990s, Science, 304, 555–559, doi:10.1126/science.1094917, 2004.

Johnson, K. M., Wills, K. D., Butler, D. B., Johnson, W. K., and Wong, C. S.: Coulometric total carbon dioxide analysis for marine studies: maximizing the performance of an automated gas extraction system and coulometric detector, Mar. Chem., 44, 167–187, doi:10.1016/0304-4203(93)90201-X, 1993.

Jones, D. C., Ito, T., Takano, Y., and Hsu, W.-C.: Spatial and seasonal variability of the air-sea equilibration timescale of carbon dioxide, Glob. Biogeochem. Cy., 28, 1163–1178, doi:10.1002/2014GB004813, 2014.

Khatiwala, S., Tanhua, T., Mikaloff Fletcher, S., Gerber, M., Doney, S. C., Graven, H. D., Gruber, N., McKinley, G. A., Murata, A., Ríos, A. F., and Sabine, C. L.: Global ocean storage of anthropogenic carbon, Biogeosciences, 10, 2169–2191, doi:10.5194/bg-10-2169-2013, 2013.

Kieke, D., Rhein, M., Stramma, L., Smethie, W. M., Bullister, J. L., and LeBel, D. A.: Changes in the pool of Labrador Sea Water in the subpolar North Atlantic, Geophys. Res. Lett., 34, L06605, doi:10.1029/2006GL028959, 2007.

Koltermann, K. P., Pfannkuche, O., and Meincke, J.: JGOFS, OMEX and WOCE in the North Atlantic 1994, cruise no. 30: 7 September to 22 December 1994, Meteor-Berichte, 96-3, Universität Hamburg, Hamburg, 148 pp., 1996.

Langdon, C., Takahashi, T., Sweeney, C., Chipman, D., Goddard, J., Marubini, F., Aceves, H., Barnett, H., and Atkinson, M. J.: Effect of calcium carbonate saturation state on the calcification rate of an experimental coral reef, Global Biogeochem. Cy., 14, 639–654, doi:10.1029/1999GB001195, 2000.

Lauvset, S. K., Gruber, N., Landschützer, P., Olsen, A., and Tjiputra, J.: Trends and drivers in global surface ocean pH over the past 3 decades, Biogeosciences, 12, 1285–1298, doi:10.5194/bg-12-1285-2015, 2015.

Lazier, J., Hendry, R., Clarke, A., Yashayaev, I., and Rhines, P.: Convection and restratification in the Labrador Sea, 1990–2000, Deep-Sea Res. Pt. I, 49, 1819–1835, doi:10.1016/S0967-0637(02)00064-X, 2002.

Le Quéré, C., Moriarty, R., Andrew, R. M., Canadell, J. G., Sitch, S., Korsbakken, J. I., Friedlingstein, P., Peters, G. P., Andres, R. J., Boden, T. A., Houghton, R. A., House, J. I., Keeling, R. F., Tans, P., Arneth, A., Bakker, D. C. E., Barbero, L., Bopp, L., Chang, J., Chevallier, F., Chini, L. P., Ciais, P., Fader, M., Feely, R. A., Gkritzalis, T., Harris, I., Hauck, J., Ilyina, T., Jain, A. K., Kato, E., Kitidis, V., Klein Goldewijk, K., Koven, C., Landschützer, P., Lauvset, S. K., Lefèvre, N., Lenton, A., Lima, I. D., Metzl, N., Millero, F., Munro, D. R., Murata, A., Nabel, J. E. M. S., Nakaoka, S., Nojiri, Y., O'Brien, K., Olsen, A., Ono, T., Pérez, F. F., Pfeil, B., Pierrot, D., Poulter, B., Rehder, G., Rödenbeck, C., Saito, S., Schuster, U., Schwinger, J., Séférian, R., Steinhoff, T., Stocker, B. D., Sutton, A. J., Takahashi, T., Tilbrook, B., van der Laan-Luijkx, I. T., van der Werf, G. R., van Heuven, S., Vandemark, D., Viovy, N., Wiltshire, A., Zaehle, S., and Zeng, N.:

Global Carbon Budget 2015, Earth Syst. Sci. Data, 7, 349–396, doi:10.5194/essd-7-349-2015, 2015.

Lherminier, P., Mercier, H., Gourcuff, C., Alvarez, M., Bacon, S., and Kermabon, C.: Transports across the 2002 Greenland-Portugal Ovide section and comparison with 1997, J. Geophys. Res., 112, C07003, doi:10.1029/2006JC003716, 2007.

Lherminier, P., Mercier, H., Huck, T., Gourcuff, C., Perez, F. F., Morin, P., Sarafanov, A., and Falina, A.: The Atlantic Meridional Overturning Circulation and the subpolar gyre observed at the A25-OVIDE section in June 2002 and 2004, Deep-Sea Res. Pt. I, 57, 1374–1391, doi:10.1016/j.dsr.2010.07.009, 2010.

Liu, X., Patsavas, M. C., and Byrne, R. H.: Purification and Characterization of meta-Cresol Purple for Spectrophotometric Seawater pH Measurements, Environ. Sci. Technol., 45, 4862–4868, doi:10.1021/es200665d, 2011.

Maier-Reimer, E. and Hasselmann, K.: Transport and storage of CO_2 in the ocean—an inorganic ocean-circulation carbon cycle model, Clim. Dynam., 2, 63–90, doi:10.1007/BF01054491, 1987.

Matear, R. J. and Lenton, A.: Quantifying the impact of ocean acidification on our future climate, Biogeosciences, 11, 3965–3983, doi:10.5194/bg-11-3965-2014, 2014.

Mehrbach, C., Culberson, C. H., Hawley, J. E., and Pytkowicz, R. M.: Measurement of the apparent dissociation constants of carbonic acid in seawater at atmospheric pressure, Limnol. Oceanogr., 18, 897–907, doi:10.4319/lo.1973.18.6.0897, 1973.

Meincke, J. and Becker, G.: WOCE-NORD, Cruise No. 18, 2 September to 26 September 1991, Nordsee, cruise No. 19, 30 September to 12 October 1991, METEOR-Berichte 93-1, Universität Hamburg, Hamburg, 105 pp., 1993.

Mercier, H., Lherminier, P., Sarafanov, A., Gaillard, F., Daniault, N., Desbruyères, D., Falina, A., Ferron, B., Gourcuff, C., and Huck, T.: Variability of the meridional overturning circulation at the Greenland–Portugal OVIDE section from 1993 to 2010, Prog. Oceanogr., 132, 250–261, doi:10.1016/j.pocean.2013.11.001, 2015.

Millero, F. J., Zhang, J. Z., Lee, K., and Campbell, D. M.: Titration alkalinity of seawater, Mar. Chem., 44, 153–165, doi:10.1016/0304-4203(93)90200-8, 1993.

Mintrop, L., Pérez, F. F., González-Dávila, M., Santana-Casiano, J. M., and Körtzinger, A.: Alkalinity determination by potentiometry: Intercalibration using three different methods, Cienc. Mar., 26, 23–37, doi:10.7773/cm.v26i1.573, 2000.

Olafsson, J., Olafsdottir, S. R., Benoit-Cattin, A., Danielsen, M., Arnarson, T. S., and Takahashi, T.: Rate of Iceland Sea acidification from time series measurements, Biogeosciences, 6, 2661–2668, doi:10.5194/bg-6-2661-2009, 2009.

Olafsson, J., Olafsdottir, S. R., Benoit-Cattin, A., and Takahashi, T.: The Irminger Sea and the Iceland Sea time series measurements of sea water carbon and nutrient chemistry 1983–2008, Earth Syst. Sci. Data, 2, 99–104, doi:10.5194/essd-2-99-2010, 2010.

Olsen, A., Abdirahman, O. M., Bellerby, R. G., Johannessen, T., Ninnemann, U. S., Brown, K. R., Olsson, K. A., Olafsson, J., Nondal, G., Kivimäe, C., Kringstad, S., Neill, C., and Olafsdottir, S.: Magnitude and Origin of the Anthropogenic CO_2 Increase and the ^{13}C Suess Effect in the Nordic Seas since 1981, Global Biogeochem. Cy., 20, GB3027, doi:10.1029/2005GB002669, 2006.

Olsen, A., Key, R. M., van Heuven, S., Lauvset, S. K., Velo, A., Lin, X., Schirnick, C., Kozyr, A., Tanhua, T., Hoppema, M., Jutterström, S., Steinfeldt, R., Jeansson, E., Ishii, M., Pérez, F. F., and Suzuki, T.: An internally consistent data product for the world ocean: the Global Ocean Data Analysis Project, version 2 (GLODAPv2), Earth Syst. Sci. Data Discuss., doi:10.5194/essd-2015-42, in review, 2016.

Ono, T., Watanabe, S., Okuda, K., and Fukasawa, M.: Distribution of total carbonate and related properties in the North Pacific along 30° N, J. Geophys. Res.-Oceans, 103, 30873–30883, doi:10.1029/1998JC900018, 1998.

Orr, J. C.: Recent and future changes in ocean carbonate chemistry, in: Ocean Acidification, Vol. 1, edited by: Gattuso, J.-P. and Hansson, L., Oxford University Press, 41–66, 2011.

Paillet, J., Arhan, M., and McCartney, M. S.: Spreading of Labrador Sea Water in the eastern North Atlantic, J. Geophys. Res., 103, 10223–10239, doi:10.1029/98JC00262, 1998.

Pérez, F. F. and Fraga, F.: A precise and rapid analytical procedure for alkalinity determination, Mar. Chem., 21, 169–182, doi:10.1016/0304-4203(87)90037-5, 1987.

Pérez, F. F., Vázquez-Rodríguez, M., Louarn, E., Padín, X. A., Mercier, H., and Ríos, A. F.: Temporal variability of the anthropogenic CO_2 storage in the Irminger Sea, Biogeosciences, 5, 1669–1679, doi:10.5194/bg-5-1669-2008, 2008.

Pérez, F. F., Vázquez-Rodríguez, M., Mercier, H., Velo, A., Lherminier, P., and Ríos, A. F.: Trends of anthropogenic CO2 storage in North Atlantic water masses, Biogeosciences, 7, 1789–1807, doi:10.5194/bg-7-1789-2010, 2010.

Pérez, F. F., Mercier, H., Vázquez-Rodríguez, M., Lherminier, P., Velo, A., Pardo, P. C., Rosón, G., and Ríos, A. F.: Atlantic Ocean CO_2 uptake reduced by weakening of the meridional overturning circulation, Nat. Geosci., 6, 146–152, doi:10.1038/ngeo1680, 2013.

Pickart, R. S., Straneo, F., and Moore, G. K.: Is Labrador Sea Water formed in the Irminger basin?, Deep-Sea Res. Pt. I, 50, 23–52, doi:10.1016/S0967-0637(02)00134-6, 2003.

Piron, A., Thierry, V., Mercier, H., and Caniaux, G.: Argo float observations of basin-scale deep convection in the Irminger sea during winter 2011–2012, Deep-Sea Res. Pt. I, 109, 76–90, doi:10.1016/j.dsr.2015.12.012, 2016.

Pörtner, H. O., Langenbuch, M., and Reipschläger, A.: Biological Impact of Elevated Ocean CO_2 Concentrations: Lessons from Animal Physiology and Earth History, J. Oceanogr., 60, 705–718, doi:10.1007/s10872-004-5763-0, 2004.

Raven, J., Caldeira, K., Elderfield, H., Hoegh-Guldberg, O., Liss, P., Riebesell, U., Shepherd, J., Turley, C., and Watson, A.: Ocean acidification due to increasing atmospheric carbon dioxide, R. Soc. Lond. Document No. 12/05, The Royal Society, London, 2005.

Read, J. F.: CONVEX-91: water masses and circulation of the Northeast Atlantic subpolar gyre, Prog. Oceanogr., 48, 461–510, doi:10.1016/S0079-6611(01)00011-8, 2000.

Rhein, M., Fischer, J., Smethie, W. M., Smythe-Wright, D., Weiss, R. F., Mertens, C., Min, D.-H., Fleischmann, U., and Putzka, A.: Labrador Sea Water: Pathways, CFC inventory, and formation rates, J. Phys. Oceanogr., 32, 648–665, doi:10.1175/1520-0485(2002)032<0648:LSWPCI>2.0.CO;2, 2002.

Riebesell, U., Zondervan, I., Rost, B., Tortell, P. D., Zeebe, R. E., and Morel, F. M. M.: Reduced calcification of marine plankton in

response to increased atmospheric CO_2, Nature, 407, 364–367, doi:10.1038/35030078, 2000.

Ríos, A. F., Álvarez-Salgado, X. A., Pérez, F. F., Bingler, L. S., Arístegui, J., and Mémery, L.: Carbon dioxide along WOCE line A14: Water masses characterization and anthropogenic entry, J. Geophys. Res.-Oceans, 108, 3123, doi:10.1029/2000JC000366, 2003.

Ríos, A. F., Resplandy, L., García-Ibáñez, M. I., Fajar, N. M., Velo, A., Padin, X. A., Wanninkhof, R., Steinfeldt, R., Rosón, G., and Pérez, F. F.: Decadal acidification in the water masses of the Atlantic Ocean, P. Natl. Acad. Sci. USA, 112, 9950–9955, doi:10.1073/pnas.1504613112, 2015.

Sabine, C. L., Feely, R. A., Gruber, N., Key, R. M., Lee, K., Bullister, J. L., Wanninkhof, R., Wong, C. S., Wallace, D. W. R., Tilbrook, B., Millero, F. J., Peng, T.-H., Kozyr, A., Ono, T., and Rios, A. F.: The Oceanic Sink for Anthropogenic CO_2, Science, 305, 367–371, doi:10.1126/science.1097403, 2004.

Santana-Casiano, J. M., González-Dávila, M., Rueda, M.-J., Llinás, O., and González-Dávila, E.-F.: The interannual variability of oceanic CO_2 parameters in the northeast Atlantic subtropical gyre at the ESTOC site, Global Biogeochem. Cy., 21, GB1015, doi:10.1029/2006GB002788, 2007.

Sarafanov, A., Falina, A., Sokov, A., and Demidov, A.: Intense warming and salinification of intermediate waters of southern origin in the eastern subpolar North Atlantic in the 1990s to mid-2000s, J. Geophys. Res.-Oceans, 113, C12022, doi:10.1029/2008JC004975, 2008.

Sarafanov, A., Falina, A., Mercier, H., Sokov, A., Lherminier, P., Gourcuff, C., Gladyshev, S., Gaillard, F., and Daniault, N.: Mean full-depth summer circulation and transports at the northern periphery of the Atlantic Ocean in the 2000s, J. Geophys. Res., 117, C01014, doi:10.1029/2011JC007572, 2012.

Sarafanov, A., Mercier, H., Falina, A., Sokov, A., and Lherminier, P.: Cessation and partial reversal of deep water freshening in the northern North Atlantic: observation-based estimates and attribution, Tellus A, 62, 80–90, doi:10.1111/j.1600-0870.2009.00418.x, 2010.

Sarmiento, J. L., Orr, J. C., and Siegenthaler, U.: A perturbation simulation of CO_2 uptake in an ocean general circulation model, J. Geophys. Res.-Oceans, 97, 3621–3645, doi:10.1029/91JC02849, 1992.

Steinfeldt, R., Rhein, M., Bullister, J. L., and Tanhua, T.: Inventory changes in anthropogenic carbon from 1997–2003 in the Atlantic Ocean between 20° S and 65° N, Global Biogeochem. Cy., 23, GB3010, doi:10.1029/2008GB003311, 2009.

Stoll, M. H. C., van Aken, H. M., de Baar, H. J. W., and Kraak, M.: Carbon dioxide characteristics of water masses in the northern North Atlantic Ocean, Mar. Chem., 55, 217–232, doi:10.1016/S0304-4203(96)00058-8, 1996.

Thierry, V., de Boisséson, E., and Mercier, H.: Interannual variability of the Subpolar Mode Water properties over the Reykjanes Ridge during 1990–2006, J. Geophys. Res.-Oceans, 113, C04016, doi:10.1029/2007JC004443, 2008.

Uppström, L. R.: Boron/chlorinity ratio of deep-sea water from the Pacific Ocean, Deep-Sea Res., 21, 161–162, doi:10.1016/0011-7471(74)90074-6, 1974.

Vázquez-Rodríguez, M., Padin, X. A., Ríos, A. F., Bellerby, R. G. J., and Pérez, F. F.: An upgraded carbon-based method to estimate the anthropogenic fraction of dissolved CO_2 in the Atlantic Ocean, Biogeosciences Discuss., 6, 4527–4571, doi:10.5194/bgd-6-4527-2009, 2009a.

Vázquez-Rodríguez, M., Touratier, F., Lo Monaco, C., Waugh, D. W., Padin, X. A., Bellerby, R. G. J., Goyet, C., Metzl, N., Ríos, A. F., and Pérez, F. F.: Anthropogenic carbon distributions in the Atlantic Ocean: data-based estimates from the Arctic to the Antarctic, Biogeosciences, 6, 439–451, doi:10.5194/bg-6-439-2009, 2009b.

Vázquez-Rodríguez, M., Padin, X. A., Pardo, P. C., Ríos, A. F., and Pérez, F. F.: The subsurface layer reference to calculate preformed alkalinity and air–sea CO_2 disequilibrium in the Atlantic Ocean, J. Marine Syst., 94, 52–63, doi:10.1016/j.jmarsys.2011.10.008, 2012a.

Vázquez-Rodríguez, M., Pérez, F. F., Velo, A., Ríos, A. F., and Mercier, H.: Observed acidification trends in North Atlantic water masses, Biogeosciences, 9, 5217–5230, doi:10.5194/bg-9-5217-2012, 2012b.

Velo, A., Pérez, F. F., Tanhua, T., Gilcoto, M., Ríos, A. F., and Key, R. M.: Total alkalinity estimation using MLR and neural network techniques, J. Marine Syst., 111–112, 11–18, doi:10.1016/j.jmarsys.2012.09.002, 2013.

Wakita, M., Watanabe, S., Honda, M., Nagano, A., Kimoto, K., Matsumoto, K., Kitamura, M., Sasaki, K., Kawakami, H., Fujiki, T., Sasaoka, K., Nakano, Y., and Murata, A.: Ocean acidification from 1997 to 2011 in the subarctic western North Pacific Ocean, Biogeosciences, 10, 7817–7827, doi:10.5194/bg-10-7817-2013, 2013.

Wallace, W. R.: Storage and transport of excess CO_2 in the oceans: The JGOFS/WOCE global CO_2 survey, in: Ocean Circulation and Climate, edited by: Siedler, G., Church, J., and Gould J., Academic Press, 489–521, 2001.

Waugh, D. W., Hall, T. M., McNeil, B. I., Key, R., and Matear, R. J.: Anthropogenic CO_2 in the oceans estimated using transit time distributions, Tellus B, 58, 376–389, doi:10.1111/j.1600-0889.2006.00222.x, 2006.

Yashayaev, I.: Hydrographic changes in the Labrador Sea, 1960–2005, Prog. Oceanogr., 73, 242–276, doi:10.1016/j.pocean.2007.04.015, 2007.

Yashayaev, I. and Dickson, R.R.: Transformation and fate of overflows in the Northern North Atlantic, in: Arctic-Subarctic Ocean Fluxes: Defining the Role of the Northern Seas in Climate, edited by: Dickson, R. R., Jens, M., and Rhines, P., Springer, Science + Business Media B.V., Dordrecht, the Netherlands, 505–526, 2008.

Yashayaev, I., Bersch, M., and van Aken, H. M.: Spreading of the Labrador Sea Water to the Irminger and Iceland basins, Geophys. Res. Lett., 34, L10602, doi:10.1029/2006GL028999, 2007.

Yashayaev, I., Holliday, N. P., Bersch, M., and van Aken, H. M.: The History of the Labrador Sea Water: Production, Spreading, Transformation and Loss, in: Arctic–Subarctic Ocean Fluxes: Defining the Role of the Northern Seas in Climate, edited by: Dickson, R. R., Meincke, J., and Rhines, P., Springer, the Netherlands, 569–612, 2008.

Zunino, P., Pérez, F. F., Fajar, N. M., Guallart, E. F., Ríos, A. F., Pelegrí, J. L., and Hernández-Guerra, A.: Transports and budgets of anthropogenic CO_2 in the tropical North Atlantic in 1992–1993 and 2010–2011, Global Biogeochem. Cy., 29, 1075–1091, doi:10.1002/2014GB005075, 2015.